

DDPM-Polycube: A Denoising Diffusion Probabilistic Model for Polycube-Based Hexahedral Mesh Generation and Volumetric Spline Construction

Yuxuan Yu^{*a}, Yuzhuo Fang^a, Hua Tong^b, Jiashuo Liu^a, Yongjie Jessica Zhang^{*b}

^a*Institute of Artificial Intelligence, Donghua University, 2999 North Renmin Road, Shanghai, 201620, China*

^b*Department of Mechanical Engineering, Carnegie Mellon University, 5000 Forbes Ave, Pittsburgh, 15213, PA, USA*

Abstract

In this paper, we propose DDPM-Polycube, a generative polycube creation approach based on denoising diffusion probabilistic models (DDPM) for generating high-quality hexahedral (hex) meshes and constructing volumetric splines. Unlike DL-Polycube methods that rely on predefined polycube structure templates, DDPM-Polycube models the deformation from input geometry to its corresponding polycube structures as a denoising task. By learning the deformation characteristics of simple geometric primitives (a cube and a cube with a hole), the DDPM-Polycube model progressively reconstructs polycube structures from input geometry by removing non-standard Gaussian noise. Once valid polycube structures are generated, they are used for surface segmentation and parametric mapping to generate high-quality hex meshes. Truncated hierarchical B-splines are then applied to construct volumetric splines that satisfy the requirements of isogeometric analysis (IGA). Experimental results demonstrate that DDPM-Polycube model can directly generate polycube structures from input geometries, even when the topology of these geometries falls outside its trained range. This provides greater generalization and adaptability for diverse engineering geometries. Overall, this research shows the potential of diffusion models in advancing mesh generation and IGA applications.

Keywords: Polycube method, Diffusion models, Generative modeling, Deep learning, Hexahedral mesh generation, Volumetric splines, Isogeometric analysis

1. Introduction

Isogeometric analysis (IGA) [1] has undergone substantial development over the past twenty years. However, the construction of volumetric parameterization remains an ongoing challenge. The approaches for construction of volumetric parameterization in IGA can be divided into two primary categories based on the input models: constructive solid geometry (CSG) [2] and boundary representation (B-Rep) [3, 4]. However, CSG-based models pose difficulties for IGA due to the presence of trimming surfaces [2]. B-Rep models require the generation of the control meshes and the construction of volumetric spline basis functions on the control meshes. In finite element analysis, B-Rep models are typically discretized into tetrahedral or hexahedral (hex) meshes. While tetrahedral meshes are widely used in industry due to the availability of multiple automatic generation strategies. Hex meshes are preferred for their advantages. These include requiring fewer elements to achieve the same level of accuracy [5], avoiding the locking issues associated with tetrahedral meshes [6], and providing better compatibility with tensor-product spline construction.

While there has been considerable progress in hex mesh generation [7, 8, 9], it is challenging to generate high-quality hex meshes for complex B-Rep models. Various methods have been explored, including indirect methods [10], sweeping methods [11, 12], grid-based methods [13, 14, 15], polycube methods [16, 17, 18, 19, 20], and vector field-based meth-

ods [21, 22]. However, not all of these methods are suitable for generating control meshes for IGA, which are used for constructing splines. Hex meshes often contain extraordinary edges and extraordinary points. When extraordinary points and extraordinary edges are involved, achieving optimal convergence rates becomes a challenging task in IGA. Therefore, among the various available methods, those that can generate meshes with as few extraordinary points and extraordinary edges as possible are preferred. In this context, sweeping and polycube methods are preferred for generating hex control meshes for IGA. Sweeping methods generate hex meshes by scanning from source to target surfaces, but their applicability is limited to models with compatible topologies between the source and target surfaces. Polycube methods generate hex meshes by using polycube structures as parameter spaces, along with parametric mapping. The methods were initially used as a texture mapping technique [16]. Lin *et al.* [23] developed an automated method for constructing polycubes; however, this method is not well-suited for models with complex topology. One of the key advantages of the polycube method is its ability to control the number and placement of extraordinary points and edges. As a result, this concept has been further extended for use in hex mesh generation. Hu *et al.* [19, 24, 20] employed centroidal Voronoi tessellation to segment surfaces. The structure of the polycube can be defined using the segmentation information, which is then used to generate hex control meshes through parametric mapping. Guo *et al.* [25] modified the polycube structure by introducing extraordinary edges to enhance

mesh quality. Li *et al.* [26] introduced the generalized polycube method, significantly expanding the adaptability of polycube techniques to high-genus and complex B-Rep models.

Constructing splines on hex control meshes is another challenge. Techniques like NURBS [11], T-splines [17, 4, 18], and TH-splines [27] have been developed for volumetric parameterization. T-splines support highly localized refinement. The truncation mechanism in TH-splines helps reduce the overlap of basis functions from different levels, thereby improving numerical conditioning. In addition, other researchers have also explored advancements in local refinement. For instance, Xu *et al.* [28] optimized control point positions in regions with significant geometric features using an r-adaptive framework. Li *et al.* [26] used the local refinement capability of T-splines to reduce geometric errors in surface fitting.

Recent efforts in artificial intelligence have affected mesh generation. MeshGPT [29] uses a decoder-only transformer to generate triangular meshes. For tetrahedral mesh generation, the DefTet [30] achieves high-quality tetrahedral reconstruction through optimization of vertex distribution and volumetric occupancy. The MeshAnything [31] framework generates triangular meshes from point clouds. In addition to triangular and tetrahedral meshes, Tong *et al.* [32] integrates the advancing front method with neural networks to generate planar unstructured quadrilateral meshes. For hex mesh generation, Yu *et al.* [33] integrates deep learning with the polycube method to generate hex control meshes for IGA. By utilizing a deep neural network, the algorithm directly predicts polycube structures, eliminating the need for traditional heuristic adjustments and additional post-processing steps. However, to enable the model to predict the ideal polycube structures, the algorithm requires as much training data as possible to cover the variability of design parameters and topologies. Generating all possible polycube structures would be an enormous task. Fortunately, polycube structures have a key characteristic: they can be decomposed into genus-0 and genus-1 geometries. Therefore, using generative models appears to be a feasible approach. By training generative models, it is possible to generate these two primitive geometries and then combine them into more complex polycube structures. This approach has the potential to improve efficiency and enhance the model's generalization ability, enabling it to better predict and generate ideal polycube structures.

Generative models can be categorized into five main types. The first type is sequence-to-sequence models [34], which belong to autoregressive decoders. These models generate sequence elements step by step and are widely used in natural language processing and time-series generation tasks. The second type is generative adversarial network models (GAN) [35], which do not explicitly model the target distribution. Instead, through adversarial training between the generator and discriminator, GANs enable the generator to produce samples that approximate the target distribution. The third type is flow-based models [36, 37], which follow a fully reversible generative process and allow direct modeling of data distributions. However, their performance is limited by the need for carefully designed structures. The fourth type is variational autoencoders

(VAE) [38], which introduce latent variables and optimize reconstruction errors, enabling the generation of diverse and continuous samples. The fifth type is diffusion models [39, 40], which share certain similarities with VAEs. The core idea of diffusion models is to learn the data distribution through a process of gradually adding and removing noise. Diffusion models have demonstrated significant advantages in various generative tasks in recent years. Ho *et al.* [40] proposed denoising diffusion probabilistic models, which iteratively learn the reverse diffusion process to generate high-quality images. These models outperform GANs [35] and VAEs [38] in terms of sample quality and stability. Unlike the adversarial training of GANs, diffusion models adopt maximum likelihood estimation, ensuring the stability of the training process and avoiding issues such as mode collapse. Song *et al.* [41] further introduced a score-based generative framework. This model improves the stability of training by mapping the generation process to stochastic differential equations. Nichol *et al.* [42] showed that by gradually denoising, diffusion models can effectively reduce the interference of noise and outliers during the generation process, thereby improving the quality of model generation.

In this paper, we introduce a novel method to generate high-quality hex meshes and construct volumetric splines by leveraging denoising diffusion probabilistic model (DDPM) and polycube techniques. Building upon the foundation of DDPM, we present the DDPM-Polycube algorithm, which utilizes diffusion models to generate polycube structures. Then the method segments geometry surfaces to match the polycube structure and generate hex meshes through parametric mapping. In summary, this paper presents four main contributions:

1. We propose an innovative perspective that the deformation from input geometry to polycube structures can be viewed as a denoising task. In this context, any input geometries are seen as polycube structures with many small-scale deformations superimposed. These deformations follow a non-standard Gaussian distribution. The algorithm employs a parameterized Markov chain to reverse the diffusion process, deforming the input geometry to polycube structures. The polycube structure generated by this process is then used for hex mesh generation and volumetric spline construction.
2. We have proposed a novel diffusion and reverse diffusion process equation specifically designed for hex mesh generation and volumetric spline construction. Our model is unique in its ability to handle non-standard Gaussian distribution, distinguishing it from many traditional diffusion models. This requires modifying the model to incorporate additional parameters and adjustments. By leveraging these enhancements, our method ensures that the reverse diffusion process generates the polycube structures. This innovation broadens the application scope of diffusion models in computational geometry and computational mechanics.
3. The DDPM-Polycube method differs from the DL-Polycube classification [33] by using diffusion models to

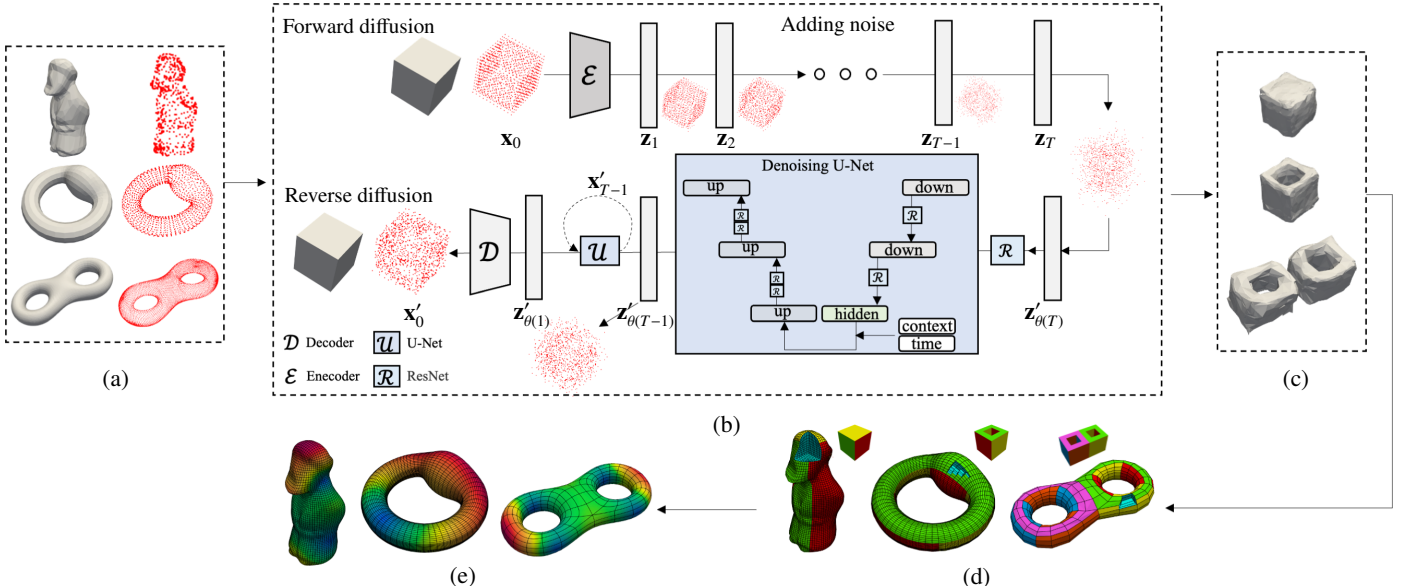


Figure 1: The DDPM-PolyCube pipeline. (a) Converting CAD geometries into triangular meshes and point clouds; (b) the DDPM-PolyCube model; (c) the polycube structure generated by the DDPM-PolyCube model; (d) an all-hex control mesh generated through octree subdivision, parametric mapping and quality improvement techniques, some elements are removed to show the interior; and (e) volumetric spline with IGA simulation results using ANSYS-DYNA. The diffusion model relies on two substeps: (1) a forward diffusion process that adds non-standard Gaussian noise to the point cloud data of the polycube structure, and (2) a reverse diffusion process that removes the noise to reconstruct the polycube structure.

construct polycube structures directly. Unlike the DL-polycube methods, which focus on learning mappings and are restricted by the ground truth structures in the dataset, the DDPM-PolyCube method focuses on learning the deformation, thereby improving the model’s generalization ability. It is particularly effective considering the wide variety of polycube structures found in real-world engineering geometries.

- Unlike traditional polycube methods, DDPM-polycube does not require additional post-processing steps and heuristic operations to ensure valid structures [7], as our DDPM-polycube algorithm leverages a diffusion model to directly generate polycube structures. Then, it performs surface segmentation (labeling) based on these predictions. Since the segmentation or labeling is inherently based on polycube structures, it naturally guarantees valid polycube structures.

The remainder of this paper is organized as follows. Section 2 provides an overview of the DDPM-PolyCube algorithm design and pipeline. Section 3 details dataset generation, feature extraction and the diffusion model architecture. Section 4 discusses how polycube structures generated using diffusion models are utilized for high-quality hex mesh generation and volumetric spline construction. Section 5 presents examples that demonstrate the algorithm’s efficiency and effectiveness. Finally, Section 6 concludes the paper and suggests directions for future research.

2. Overview of the pipeline

As shown in Fig. 1, our DDPM-PolyCube pipeline begins with a triangular mesh representing the CAD geometry. Subsequently, our DDPM-PolyCube model is employed to directly generate polycube structures. This polycube structure serves as the foundation for generating all-hex meshes through surface segmentation and parametric mapping [43]. To ensure that the generated all-hex mesh meets the quality requirements necessary for IGA, we employ several mesh quality improvement techniques—such as pillowing [44], smoothing, and optimization [4, 13, 45]—as needed. Upon achieving a high-quality hex mesh, the volumetric spline model is constructed from these meshes using TH-spline3D with local refinement [27, 20]. Finally, the Bézier information is extracted for performing IGA in ANSYS-DYNA.

3. DDPM-PolyCube model

As shown in Fig. 1, we propose a new DDPM-PolyCube approach, which iteratively deforms the input geometry into corresponding polycube structures. Unlike DL-PolyCube methods [33], which rely on the predefined polycube types and mapping between the input geometry and output polycube types. The DDPM-PolyCube algorithm models the geometric deformation process as a denoising task.

In the preprocessing step, the input geometries are first converted into point cloud data, which then serves as the input to the DDPM-PolyCube model. The DDPM-PolyCube model operates in two steps (see Fig. 1): (1) a forward diffusion process, where non-standard Gaussian noise is incrementally added to the point cloud data, and (2) a reverse diffusion process, where

the model progressively removes the deformation to recover the target polycube structure. During the training step, the model learns the deformation capability from simple geometric primitives: a cube and a cube with a hole. Once training is complete, the model generalizes to more complex geometries. The DDPM-Polycube algorithm consists of data generation, feature extraction, and training the improved DDPM model. These steps work together to generate polycube structures from input geometries.

3.1. Data generation

In the data generation step, we focus on creating a context-rich dataset starting from two basic geometric primitives: a cube (genus-0) and a cube with a hole (genus-1). These models are generated and discretized into triangular meshes using the 3D graphics software Blender, along with its built-in Python and BMesh libraries. To provide additional contextual information, we further assign these geometric primitives to specific positions and treat geometric primitives at different positions as different types. As shown in Fig. 2, the first 8 columns are composed of single geometric primitive, while the 9th column contains a combination of two geometric primitives. Note that the cube with a hole is further categorized based on the axis along which the hole is oriented (X -axis, Y -axis, or Z -axis), resulting in two additional variations. To assign the positions of these geometric primitives, we design a 2×1 grid $G_{2 \times 1}$. The $G_{2 \times 1}$ grid consists of two units arranged in one column with two rows (see Fig. 2 for an illustration of the grid for each type of geometric configurations).

To enable the DDPM-Polycube model to learn more complex structures, we introduce a 9th type, represented by the 9th column shown in Fig. 2. This type consists of two cubes and occupy two units of the $G_{2 \times 1}$ grid. One cube is placed on the top of the other. The inclusion of this composite geometric configuration type is essential to help the DDPM-Polycube model understand that polycube structures can be formed by combining multiple geometric primitives. Our experiments show that without this 9th type, the model fails to learn the ability to combine geometric primitives effectively. As a result, it can only generate a single cube or a cube with a hole, and fails to generate more complex polycube structures composed of multiple geometric primitives.

To contextualize these types, we use a one-hot encoding scheme, a common method for representing discrete features. This encoding assigns a unique binary vector to each type, where the vector's length is 29, and each bit indicates the presence or absence of a specific geometric type or combination. For geometric primitives types (the first 8 types), each type occupies a distinct position in the one-hot encoding vector, and the corresponding bit is set to 1 to indicate its presence. For the 9th composite type, two positions in the vector are activated simultaneously to indicate the presence of two geometric primitives. The encoding rules are as follows: for the first 8 types, $\text{context} = \delta_{n,4T}, t = 0, 1, \dots, 7$; for the 9th type, $\text{context} = \delta_{n,0} + \delta_{n,4}$, where n represents the position, δ is the Kronecker delta, and T represents the geometric type. Through this encoding method, each type of geometric configuration is

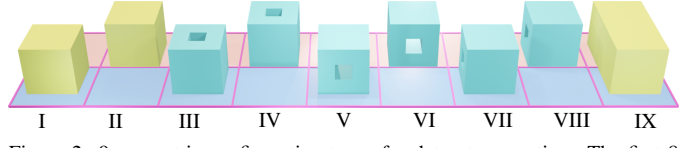


Figure 2: 9 geometric configuration types for dataset generation. The first 8 columns contain one geometric primitive, either a cube or a cube with a hole oriented along the Z , X , or Y axis, placed in different positions. The 9th column represents composite structures formed by two primitives. These configurations, along with the one-hot encoding, provide the starting point for the forward diffusion process.

uniquely represented, enabling the model to recognize and learn from them effectively.

With these 9 types of geometric configurations, we can generate a context-aware dataset. For each of those 9 types of geometric configurations, we introduce non-standard Gaussian noise to these geometries. This noise can be interpreted as small-scale deformations that progressively obscure the original polycube structure. By applying this noise, we generate a series of deformed geometry, forming a class of latent variable models. Finally, the dataset is used for the reverse diffusion process, enabling the model to learn the ability to generate polycube structures by gradually deforming (denoising) the input geometry.

3.2. Feature extraction

The feature extraction process begins by converting the triangular mesh into a point cloud, denoted as $P = \{\mathbf{p}_1, \mathbf{p}_2, \dots, \mathbf{p}_N\}$, where each point $\mathbf{p}_i = \mathbf{x}_i$ represents the 3D coordinates of the i -th point, with $\mathbf{x}_i = (x_i, y_i, z_i)$. Here, N is the total number of points. The 3D coordinates of the point cloud are then normalized to the range $[-1, 1]$. After normalization, the coordinates are further scaled to the range $[-0.5, 0.5]$ and then shifted by 0.5 along the X -axis. Subsequently, all data are sorted along the X -axis. For the first eight types of geometric configurations (the first eight columns shown in Fig. 2), each type occupies one unit in the $G_{2 \times 1}$ grid and contains 512 points. To ensure consistent data size across all geometric configurations, an additional 512 zeros are appended to these 512 points, resulting in a total of 1,024 points for each geometric configuration. For polycube structure that occupy two units in the $G_{2 \times 1}$ grid (the 9th column shown in Fig. 2), it contains 1,024 points without the need for zero padding. Regardless of the number of units occupied in the $G_{2 \times 1}$ grid, the point clouds of all geometric configurations are processed and organized into a three-channel 32×32 matrix. This process maps the points of the triangular mesh into a 32×32 matrix, creating images that serve as inputs for the DDPM-Polycube model. By leveraging image-like data structures, this method aligns with the DDPM framework.

During the reverse diffusion process, the input geometry is considered as x'_T and requires normalization to ensure consistency with the dataset's scale. It is then converted into a three-channel 32×32 matrix using the same data structure of the training data, serving as the input for the reverse diffusion process. Then, the result generated by the reverse diffusion process is in three-channel 32×32 matrix. These need to be decoded back into 3D coordinates. Finally, the generated point cloud

data maintains the same number of points as the vertices of the original triangular mesh and has the same topology.

Remark 1 (Training data design). *The training data for the DDPM-PolyCube algorithm includes nine types, based on two geometric primitives (a cube and a cube with a hole) and a combination of two cubes. While these two geometric primitives form the foundation, other basic geometric primitives can also be included. The combination configuration helps the model learn how geometric primitives merge, enabling it to reconstruct more complex structures.*

Remark 2 (Grid configuration design). *This study uses a simplified 2×1 grid configuration as a proof-of-concept to reduce complexity. Despite the limited dataset, the results show the model can generalize effectively, deforming complex CAD geometries into polycube structures, even for topologies beyond its training range. The algorithm is also extensible, supporting larger grid configurations such as a 3×2 grid, $m \times n$ grids, or even higher-dimensional grids. This would enable it to handle more complex geometries and topologies.*

3.3. DDPM-PolyCube model architecture

The improved DDPM plays a key role in DDPM-PolyCube model, enabling the deformation and reconstruction of corresponding polycube structures. It operates through two diffusion processes: the forward diffusion process and the reverse diffusion process. In the forward diffusion process, non-standard Gaussian noise is progressively added to the polycube structure (as shown in Fig. 1), gradually deforming it into a geometry with a Gaussian noise. The reverse diffusion process iteratively removes the deformation, reconstructing the corresponding polycube structure step by step through deformation (denoising).

3.3.1. Forward diffusion process

The forward diffusion process is a Markov chain that progressively corrupts the polycube structure \mathbf{x}_0 by introducing non-standard Gaussian noise at each timestep t . Using the reparameterization trick, the non-standard Gaussian noise $\mathcal{N}(\mathbf{q}, I)$ is reformulated as the sum of standard Gaussian noise $\mathcal{N}(0, I)$ and the adjustment term \mathbf{q} . Consequently, the geometry at timestep t is expressed as:

$$\mathbf{x}_t = \sqrt{\alpha_t} \mathbf{x}_{t-1} + \sqrt{1 - \alpha_t} (\mathbf{z}_{t-1} + \mathbf{q}), \quad \mathbf{z}_t \sim \mathcal{N}(0, I), \quad (1)$$

where \mathbf{x}_t represents the deformed geometry at timestep t , $\alpha_t = 1 - \beta_t$, and β_t is a predefined deformation schedule. The term \mathbf{z}_t denotes standard Gaussian noise, and \mathbf{q} is a new term introduced in this paper that differentiates this method from the standard DDPM framework [40].

To further simplify the forward diffusion process, we reformulate Equation (1) in terms of \mathbf{x}_0 and \mathbf{q} . This reformulation enables the computation of \mathbf{x}_t for any timestep t without requiring intermediate iterations or latent variable models. By leveraging the reparameterization trick, the forward diffusion

process can be expressed as:

$$\begin{aligned} \mathbf{x}_t &= \sqrt{\alpha_t} \mathbf{x}_{t-1} + \sqrt{1 - \alpha_t} (\mathbf{z}_{t-1} + \mathbf{q}) \\ &= \sqrt{\alpha_t} \left(\sqrt{\alpha_{t-1}} \mathbf{x}_{t-2} + \sqrt{1 - \alpha_{t-1}} (\mathbf{z}_{t-2} + \mathbf{q}) \right) \\ &\quad + \sqrt{1 - \alpha_t} (\mathbf{z}_{t-1} + \mathbf{q}) \\ &= \sqrt{\bar{\alpha}_t} \mathbf{x}_0 + \sqrt{1 - \bar{\alpha}_t} \bar{\mathbf{z}}_t + \mathbf{Q}_t, \end{aligned} \quad (2)$$

where $\mathbf{z}_{t-1}, \mathbf{z}_{t-2}, \dots, \sim \mathcal{N}(0, I)$, $\bar{\alpha}_t = \prod_{i=1}^t \alpha_i$ is the cumulative deformation decay, $\bar{\mathbf{z}}_t$ aggregates the Gaussian distribution up to timestep t , and $\mathbf{Q}_t = \left(\sum_{k=1}^t \sqrt{(1 - \alpha_k) \prod_{i=k+1}^t \alpha_i} \right) \mathbf{q}$ is a term that accounts for the cumulative influence of \mathbf{q} across all previous timesteps. From Equation (2), the conditional probability $q(\mathbf{x}_t | \mathbf{x}_0)$ can be derived as:

$$q(\mathbf{x}_t | \mathbf{x}_0) = \mathcal{N}(\mathbf{x}_t; \sqrt{\bar{\alpha}_t} \mathbf{x}_0 + \mathbf{Q}_t, (1 - \bar{\alpha}_t) I), \quad (3)$$

where the mean is scaled by $\sqrt{\bar{\alpha}_t}$, and the variance is determined by $1 - \bar{\alpha}_t$, reflecting the cumulative deformation applied up to timestep t . The inclusion of \mathbf{q} in \mathbf{Q}_t adjusts the forward diffusion process to account for the relationship between the endpoint of the forward diffusion process and the polycube structure.

Remark 3 (Non-standard Gaussian noise). *In the standard DDPM framework [40], when the timestep t approaches infinity, the data converges into a standard Gaussian distribution. However, this does not meet the requirements of our method. For the DDPM-PolyCube algorithm, the endpoint of the forward diffusion process (\mathbf{x}_T) needs to be represented as a geometry. To achieve this, we introduce a non-standard Gaussian noise, where \mathbf{q} is defined as an incremental adjustment term applied during the forward diffusion process. This adjustment term deforms the polycube structure (\mathbf{x}_0) into the final geometry (\mathbf{x}_T).*

Remark 4 (Computation of \mathbf{q}). *When the timestep t approaches infinity, \mathbf{x}_t converges to $\bar{\mathbf{z}}_t + \mathbf{Q}_t$, as described in Equation (2). Here, \mathbf{x}_t represents the endpoint of the forward diffusion process, which also serves as the initial state (input geometry) for the reverse diffusion process. Then, the adjustment term \mathbf{Q}_t can be calculated. Since $\mathbf{Q}_t = \left(\sum_{k=1}^t \sqrt{(1 - \alpha_k) \prod_{i=k+1}^t \alpha_i} \right) \mathbf{q}$, the value of \mathbf{q} can be directly derived.*

3.3.2. Reverse diffusion process

The reverse diffusion process aims to reconstruct the input geometry \mathbf{x}'_t to the corresponding polycube structure (\mathbf{x}'_0). By utilizing a parameterized neural network $\mathbf{z}'_\theta(\mathbf{x}'_t, t)$, \mathbf{x}'_t is iteratively deformed. This ensures that the original geometric topology is preserved while gradually generating the corresponding polycube structure. Mathematically, the reverse diffusion process is modeled as a conditional probability distribution:

$$q(\mathbf{x}'_{t-1} | \mathbf{x}'_t, \mathbf{x}'_0) = \mathcal{N}(\mathbf{x}'_{t-1}; \mu'_t(\mathbf{x}'_t, \mathbf{x}'_0), \sigma_t^2 I), \quad (4)$$

where $\mu'_t(\mathbf{x}'_t, \mathbf{x}'_0)$ is the mean of the corresponding Gaussian distribution, which represents a weighted combination of \mathbf{x}'_t and

\mathbf{x}'_0 , and $\sigma_t^2 = \frac{1-\bar{\alpha}_t}{1-\bar{\alpha}_t} \beta_t$ is the variance at timestep t . By iteratively estimating this conditional distribution, the model effectively reconstructs the geometry generated during the forward process.

To compute \mathbf{x}'_{t-1} , solving for the mean μ'_t is the core step in the reverse diffusion process, as it guides the reconstruction of geometry at each timestep t . Referring to the DDPM [40] and adapting it for our polycube reconstruction task, we can get similar function:

$$\mu'_t = \frac{1}{\sqrt{\alpha_t}} \left(\mathbf{x}'_t - \frac{\beta_t}{\sqrt{1-\bar{\alpha}_t}} (\mathbf{z}'_\theta(\mathbf{x}'_t, t) + \mathbf{q}') \right). \quad (5)$$

The parameter \mathbf{q}' is an adjustment term introduced to ensure the integrity of the reconstructed polycube structure, while the neural network $\mathbf{z}'_\theta(\mathbf{x}'_t, t)$ is trained to predict the deformation added during the forward diffusion process. Compared to the equation in the literature [40], our method introduces an additional parameter \mathbf{q}' , which can be derived as follows.

To reconstruct \mathbf{x}'_{t-1} , the reverse diffusion process combines the predicted mean μ'_t with the variance term $\sigma_t \mathbf{z}'_t$, resulting in the following equation:

$$\begin{aligned} \mathbf{x}'_{t-1} &= \mu'_t + \sigma_t \mathbf{z}'_t \\ &= \frac{1}{\sqrt{\alpha_t}} \left(\mathbf{x}'_t - \frac{\beta_t}{\sqrt{1-\bar{\alpha}_t}} (\mathbf{z}'_\theta(\mathbf{x}'_t, t) + \mathbf{q}') \right) + \sigma_t \mathbf{z}'_t. \end{aligned} \quad (6)$$

By iteratively applying the reverse diffusion process across all timesteps, the target polycube structure \mathbf{x}'_0 can be progressively reconstructed. Starting from \mathbf{x}'_0 at timestep 0, the process can be expressed as:

$$\begin{aligned} \mathbf{x}'_0 &= \frac{1}{\sqrt{\alpha_1}} \left(\mathbf{x}'_1 - \frac{\beta_1}{\sqrt{1-\bar{\alpha}_1}} (\mathbf{z}_1 + \mathbf{q}') \right) + \sigma_1 \mathbf{z}'_1 \\ &= \frac{1}{\sqrt{\alpha_1}} \left(\frac{1}{\sqrt{\alpha_2}} \left(\mathbf{x}'_2 - \frac{\beta_2}{\sqrt{1-\bar{\alpha}_2}} \mathbf{q}' \right) \right) \\ &\quad - \frac{1}{\sqrt{\alpha_1}} \frac{\beta_1}{\sqrt{1-\bar{\alpha}_1}} \mathbf{q}' + \mathbf{z} \\ &= \frac{1}{\sqrt{\bar{\alpha}_t}} (\mathbf{x}'_t) + \tilde{\mathbf{z}} - \mathbf{Q}', \end{aligned} \quad (7)$$

where $\mathbf{Q}' = \sum_{k=1}^t \frac{1}{\sqrt{\bar{\alpha}_t}} \frac{\sqrt{1-\alpha_k}}{\sqrt{1-\bar{\alpha}_k}} \sqrt{1-\alpha_k} \prod_{i=k+1}^t \sqrt{\alpha_i} \mathbf{q}'$ represents the cumulative deformation adjustments across all timesteps, $\tilde{\mathbf{z}}$, derived through the reparameterization trick, aggregates the Gaussian distribution. Under ideal conditions, when $t = T$, where $\mathbf{x}_t = \mathbf{x}'_t$ and $\mathbf{x}_0 = \mathbf{x}'_0$, the value of \mathbf{q}' can be derived by combining this assumption with Equation (2). We have:

$$\sum_{k=1}^t \frac{1}{\sqrt{\bar{\alpha}_t}} \frac{\sqrt{1-\alpha_k}}{\sqrt{1-\bar{\alpha}_k}} \sqrt{1-\alpha_k} \prod_{i=k+1}^t \sqrt{\alpha_i} \mathbf{q}' = \frac{\mathbf{Q}_t}{\sqrt{\bar{\alpha}_t}}. \quad (8)$$

Then, we obtain

$$\mathbf{q}' = \frac{\sqrt{1-\bar{\alpha}_k}}{\sqrt{1-\alpha_k}} \mathbf{q}. \quad (9)$$

This indicates that the value of \mathbf{q}' depends on the timestep k and the diffusion adjustment term \mathbf{q} .

Remark 5 (Reparameterization trick). *The reparameterization trick leverages the statistical properties of Gaussian distribu-*

tions. For example, given two independent Gaussian distributions $X \sim \mathcal{N}(\mu_1, \sigma_1^2)$ and $Y \sim \mathcal{N}(\mu_2, \sigma_2^2)$, their linear combination $aX + bY$ results in a new Gaussian distribution with a mean of $a\mu_1 + b\mu_2$ and a variance of $a^2\sigma_1^2 + b^2\sigma_2^2$. This principle is applied in the DDPM-Polycube algorithm to derive the cumulative impact of \mathbf{q} and \mathbf{q}' over multiple timesteps during the forward diffusion process and the reverse diffusion process.

3.3.3. Training the DDPM-Polycube model

The training step of DDPM-Polycube focuses on training the deformation predictor $\mathbf{z}'_\theta(\mathbf{x}_t, t)$ to learn the reverse diffusion process, enabling it to predict the small-scale deformations added during the forward diffusion process. The loss function is defined as the mean squared error (MSE) between the true noise \mathbf{z} and the predicted noise $\mathbf{z}'_\theta(\mathbf{x}_t, t)$:

$$\mathcal{L} = \mathbb{E}_{\mathbf{x}_0, \mathbf{z}, t} [\|\mathbf{z} - \mathbf{z}'_\theta(\mathbf{x}_t, t)\|^2], \quad (10)$$

where \mathbf{x}_t represents the target geometry generated during the forward diffusion process according to Equation (2). By iteratively optimizing this loss function, the neural network learns to predict the deformation at each timestep, enabling effective deformed during the reverse diffusion process.

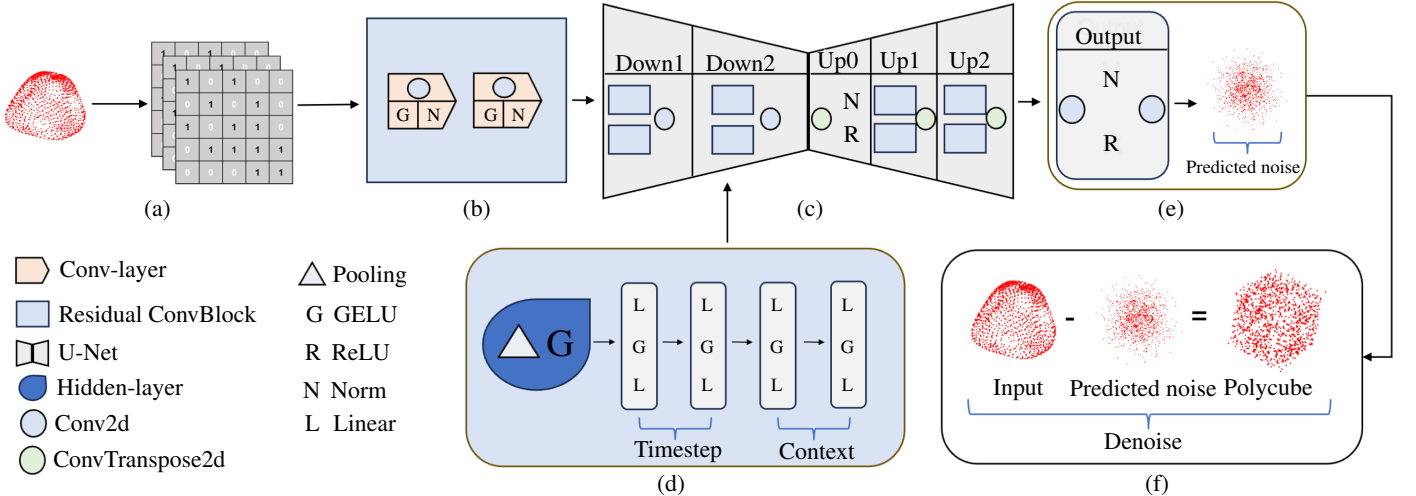
Algorithm 1 Training the DDPM-Polycube model

Require: Dataset of polycube structures $\{\mathbf{x}_0\}$, number of diffusion steps T , deformation schedule $\{\beta_t\}$
Ensure: Trained parameterized neural network $\mathbf{z}'_\theta(\mathbf{x}_t, t)$

- 1: Compute cumulative deformation coefficients: $\alpha_t = 1 - \beta_t$, $\bar{\alpha}_t = \prod_{i=1}^t \alpha_i$
- 2: **for** each training iteration **do**
- 3: Randomly sample a time step $t \sim \text{Uniform}(1, T)$
- 4: Sample standard Gaussian noise $\mathbf{z} \sim \mathcal{N}(0, I)$
- 5: Calculate \mathbf{Q}_t
- 6: Generate deformed geometry $\mathbf{x}_t = \sqrt{\bar{\alpha}_t} \mathbf{x}_0 + \sqrt{1-\bar{\alpha}_t} \mathbf{z} + \mathbf{Q}_t$ at each timestep
- 7: Using parameterized neural network $\mathbf{z}'_\theta(\mathbf{x}_t, t)$ to predict noise
- 8: Compute loss: $\mathcal{L} = \|\mathbf{z} - \mathbf{z}'_\theta(\mathbf{x}_t, t)\|^2$
- 9: Update neural network by minimizing \mathcal{L}
- 10: **end for**

During the forward diffusion process (see Algorithm 1), the polycube structure data is progressively added by the small-scale deformation, which follows a non-standard Gaussian noise. This process follows a predefined deformation schedule. In our paper, the schedule is designed linearly. It is controlled by the initial and final noise values ($\beta_1 = 1 \times 10^{-4}$, $\beta_T = 0.02$). The deformation increases gradually over time. This design ensures that earlier timesteps retain more of the original polycube structure, while later stages become increasingly dominated by large-scale deformation. Specifically, for a polycube structure \mathbf{x}_0 , the deformed geometry \mathbf{x}_t at timestep t is generated using Equation (2).

Once training is complete, the reverse diffusion process (i.e., the sampling from the DDPM-Polycube model) iteratively deforms the input geometry to reconstruct the polycube structure



Algorithm 2 Sampling from the DDPM-PolyCube model

Require: Trained parameterized neural network $\mathbf{z}'_\theta(\mathbf{x}', t)$, number of diffusion steps T , deformation schedule $\{\beta_t\}$, input geometry \mathbf{x}'_T
Ensure: Generated polycube structure \mathbf{x}'_0

- 1: **for** $t = T, T-1, \dots, 1$ **do**
- 2: Calculate \mathbf{q}'
- 3: Compute $\sigma_t = \sqrt{\beta_t}$,
- 4: Sample deformation $\mathbf{z}'_t \sim \mathcal{N}(0, I)$ if $t > 1$, otherwise $\mathbf{z}'_0 = 0$
- 5: Update sample: $\mathbf{x}'_{t-1} = \mu'_t + \sigma_t \mathbf{z}'_t$
- 6: **end for**
- 7: **return** \mathbf{x}'_0

(see Algorithm 2). Starting from the final timestep T , the model predicts the deformation at each step and uses it to compute the mean and variance of the deformation distribution. Specifically, at timestep t , the mean μ'_t (Equation (5)) and variance σ_t^2 of the non-standard Gaussian noise are calculated. By sampling from this distribution, the model progressively removes deformation at each step, ultimately generating the polycube structure.

The architecture of the DDPM-PolyCube model is built upon a U-Net framework (see Fig. 3), which includes an initial convolutional layer, two downsampling modules and two upsampling modules, as well as fully connected embedding layers for timestep and context features. The U-Net framework leverages skip connections to transfer features between the downsampling and upsampling modules. This helps preserve both geometric details and the topological structure.

Before training, the input geometry undergoes preprocessing,

including normalization, scaling, and mapping onto a three-channel 32×32 matrix to create image-like data structures compatible with the U-Net framework (see Fig. 3(a)). The initial convolutional layer (see Fig. 3(b)) is implemented as a residual convolutional block, taking three-channel geometric data as input and producing feature maps with a dimension of 64. The residual convolutional block uses GELU activation functions and batch normalization to enhance feature extraction while maintaining stability during training. The downsampling module (see Fig. 3(c)) consists of two residual convolutional blocks followed by a max-pooling layer, progressively extracting local geometric features while reducing spatial resolution. The feature dimensions increase to 128 during the downsampling module. Max-pooling reduces the spatial resolution by half, enabling the extraction of higher-level features. At the same time, the timestep and context features (see Fig. 3(d)) are embedded using fully connected layers. The timestep embedding layer takes a scalar input of dimension 1 and outputs a vector of dimension 128, while the context embedding layer takes a 29-dimensional input (see Section 3.1) and produces an output of dimension 128. These embedded features are fused with convolutional features through additive and multiplicative operations, enhancing the model’s ability to capture contextual information. Fully connected layers are used for embedding generation, with GELU activation ensuring smooth transitions across dimensions. The upsampling module (see Fig. 3(c)) consists of transposed convolutional layers combined with ReLU activation and two residual convolutional blocks. The feature dimensions are reduced from 128 back to 64, with transposed convolutional layers doubling the spatial resolution. To preserve the geometric details and topological structure, skip connections are employed to transfer features between the corresponding layers in the downsampling and upsampling modules. Finally, an output convolutional layer (see Fig. 3(e)) maps the features back to the three-channel data, producing the predicted

noise. This noise can be interpreted as small-scale deformations. By gradually removing the noise from the input geometry, the polycube structure is generated (see Fig. 3(f)).

4. Hex mesh generation and volumetric spline construction

In this section, we describe how to generate high-quality hex meshes and construct volumetric splines from the polycube structures produced by the DDPM-Polycube algorithm. While the methods used here are based on existing techniques [33, 20], we provide a concise overview to maintain the completeness of the proposed pipeline. For a detailed understanding of the algorithms and their underlying principles, we refer readers to [20, 27, 33]. The implementation of these methods has been integrated into HexGen and Hex2Spline software packages, which are publicly available on GitHub [46]. These robust tools enable users to efficiently generate high-quality hex meshes and construct volumetric splines for IGA applications.

4.1. Hex mesh generation

To generate a high-quality hex mesh, the polycube structure and its associated surface segmentation serve as the foundation. The process begins by establishing a bijective mapping between the input triangular mesh and the boundary surface of the polycube. This mapping is achieved through parametric mapping techniques, where each segmented surface patch corresponds to a boundary surface of the polycube. Utilizing the cotangent Laplace operator, we ensure that the parametric mapping is harmonic and bijective. Internal regions of the polycube are parameterized using linear interpolation. The hex mesh is constructed from this parametric mapping in conjunction with octree subdivision, where each cubic region of the polycube structure is subdivided into smaller cubes to generate volumetric mesh elements. Vertices are then mapped from the parametric domain to the physical domain. To address mesh quality issues that arise during the hex mesh generation, we integrate several quality improvement techniques, including pillowowing, smoothing, and optimization. Pillowowing improves mesh quality by inserting additional layers around the boundary. Smoothing relocates vertices to improve mesh quality while preserving geometric feature. The optimization improves the scaled Jacobian [47] by minimizing an energy function. This energy function incorporates geometry fitting and element shape metrics. By alternately applying these optimization techniques, a high-quality hex mesh is generated.

4.2. Volumetric spline construction

Following the generation of a high-quality hex mesh, the next step involves constructing volumetric splines, specifically TH-spline3D, on the unstructured hex mesh. The spline construction begins by using the hex mesh as the control mesh. The TH-spline3D framework is employed to define spline functions over the hex mesh, preserving sharp features and supporting local refinement. The constructed volumetric splines maintain C^0 continuity around extraordinary points and C^2 continuity in regular regions, ensuring smoothness and accuracy for IGA

simulations. To facilitate integration with simulation platforms, Hex2Spline [46] can export the Bézier information of the volumetric splines. This enables seamless compatibility with IGA solvers such as ANSYS-DYNA.

5. Results and discussion

5.1. Training performance of the DDPM-Polycube model

During the forward diffusion process, non-standard Gaussian noise is added to the polycube structures. The polycube structures include 9 types, as described in Section 3.1. This noise progressively corrupts the polycube structures. In the reverse diffusion process, the model predicts and removes the noise step by step. This restores the polycube structure. The training objective minimizes the MSE (see Equation (10)) between the true noise and the predicted noise at each timestep. This ensures reconstruction of the polycube structure from the input geometry. The diffusion process is configured with 500 timesteps. Increasing the number of timesteps can improve reconstruction quality but also raises computational costs. Details about the DDPM-Polycube model are provided in Section 3.3.3. The model is trained with a batch size of 200 over 400 epochs. The initial learning rate η is set to 1×10^{-3} . It is adjusted using a linear decay strategy based on the current epoch. The formula is $\eta_k = \eta_{k-1} \times (1 - \frac{k}{K})$, where η_k is the learning rate for the current epoch, k is the current epoch, and K is the total number of epochs. The Adam optimizer is used to improve training stability.

To assess the performance of the proposed DDPM-Polycube algorithm, we implemented it using Python on a system equipped with an Intel Xeon CPU, 64 GB of RAM, and an RTX 4080 GPU. Fig. 4 displays the loss function of the DDPM-Polycube model as a function of epochs, demonstrating the convergence behavior during training.

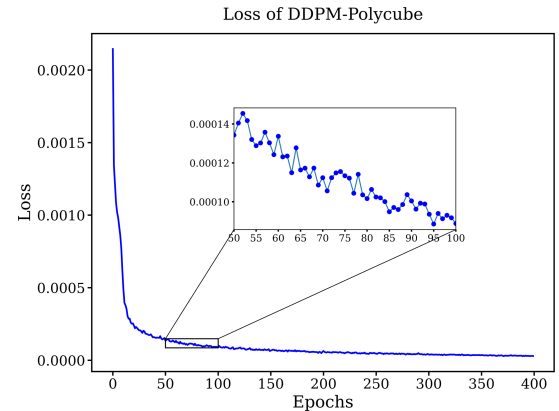


Figure 4: Loss of the DDPM-Polycube model as a function of epochs.

5.2. Performance evaluation in geometries of different genus

In this section, we evaluate the performance of the DDPM-Polycube algorithm on models with varying genus levels. The results demonstrate its ability to generate polycube structures, adapt to complex topologies, and recognize geometric topologies beyond its training range (see Figs. 5 and 6).

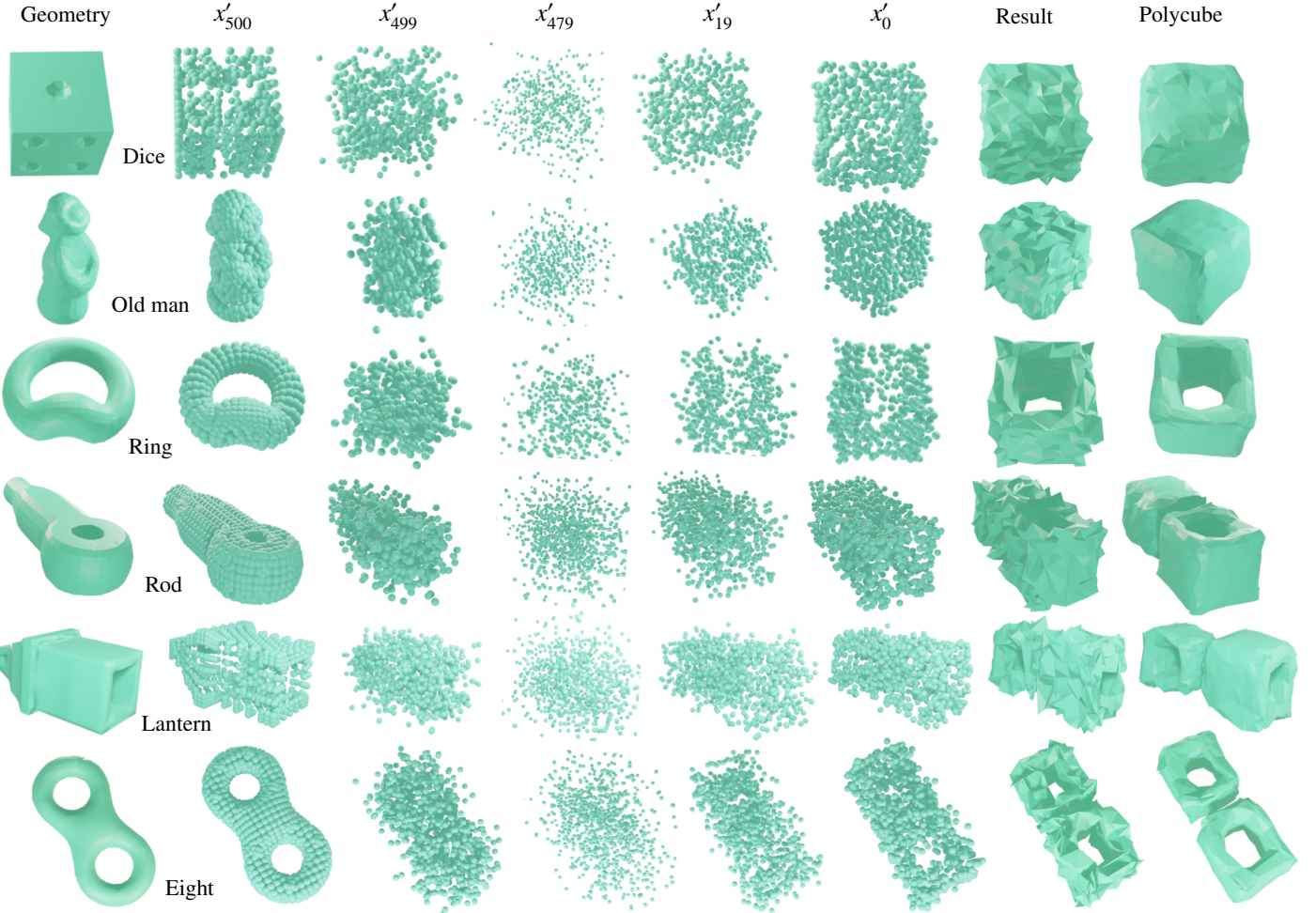


Figure 5: The DDPM-Polycube algorithm’s capability to generate polycube structures for various geometric models with different genus levels, demonstrating its ability to adapt to complex topologies and generate polycube structures beyond its training set. Examples include genus-0 models (Dice, Old man), genus-1 models (Ring, Rod, Lantern), and genus-2 models (Eight). The reverse diffusion process starts from the input geometry (x'_{500}), progresses through latent variable models (x'_{499} , x'_{479} , x'_{19}), and gradually removes the noise to reconstruct the final polycube structure (x'_0).

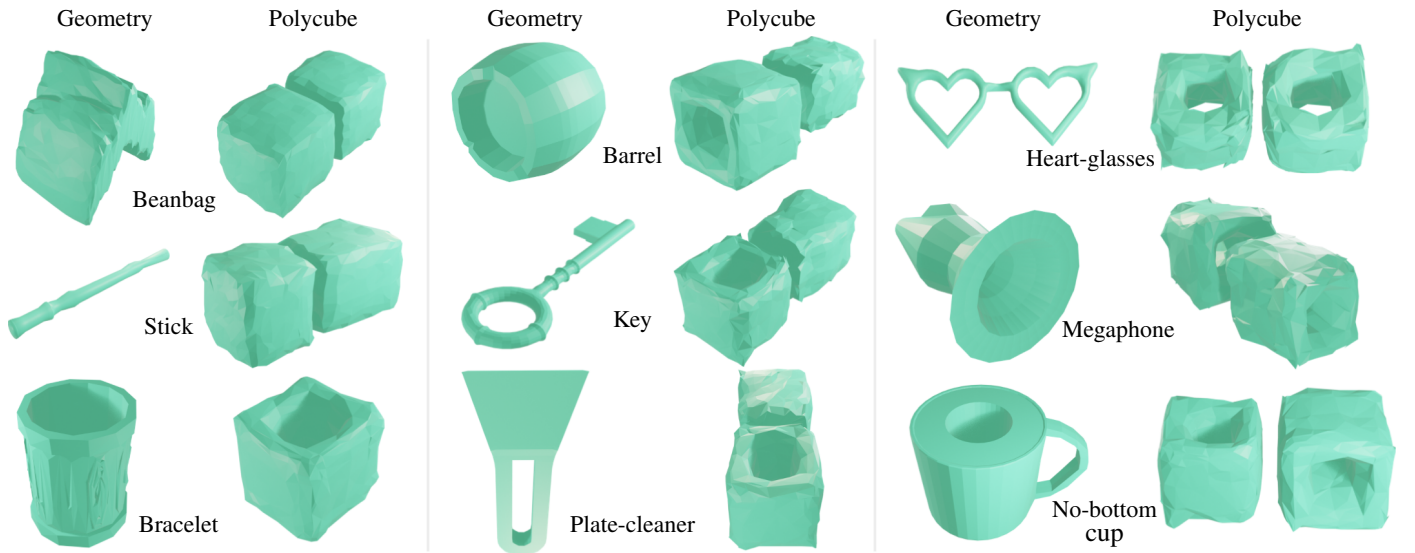


Figure 6: Additional results demonstrating the capability of the DDPM-Polycube algorithm in handling a wide range of geometric models. This includes examples of various genus-0 (Beanbag, Stick, Barrel), genus-1 (Bracelet, Key, Plate-cleaner, Megaphone), and genus-2 (Heart-glasses, No-bottom cup) structures.

Our initial tests focus on simple genus-0 and genus-1 models. Although these geometries are not part of the training set, their topology falls within the 9 geometric configuration types shown in Fig. 2. For example, the Old Man and Dice models (see Fig. 5) are reconstructed as Type I polycube structures. These models are represented as single cubes. For more complex genus-0 geometries, such as the Stick and Beanbag models (see Fig. 6), the algorithm generates Type IX polycube structures. These structures consist of two cubes. For genus-1 models, the algorithm remains effective. The Ring model (see Fig. 5) and the Bracelet model (see Fig. 6) are reconstructed as Type III polycube structures (see Fig. 2). The results confirm that the algorithm captures the deformation required to represent their polycube structures. In summary, the DDPM-Polycube algorithm successfully generates polycube structures for models with topologies similar to those from Type I to Type IX.

Now, we turn our attention to geometries whose topology falls outside the training range. For the Barrel model (see Fig. 6), which is genus-0, there are no similar topologies in the dataset. Despite this, the algorithm successfully captures the deformation and generates a valid polycube structure. The barrel falls under the category of punctured geometries. In these geometries, the presence of holes does not alter their fundamental topological properties. To match the topology of the barrel, the algorithm generates one cube and one cube with a hole. In this configuration, one cube's wall covers the hole of the other. This results in a polycube structure consistent with the barrel's topology. These results demonstrate the DDPM-Polycube algorithm's flexibility in handling punctured geometries and producing valid polycube structures.

For genus-1 models, such as the Rod (see Fig. 5) and Key (see Fig. 6) models, the algorithm successfully captures their topological features, even though no similar topologies exist in the training dataset. It deforms the upper part of these models into a cube and the lower part into a cube with a hole. Similarly, for the Lantern model (see Fig. 5), the algorithm handles the additional complexity of punctured geometries, generating a polycube structure where the wall of one cube with a hole covers another cube with a hole, while preserving the overall geometric topology. These results highlight the algorithm's ability to recognize and process punctured geometries with genus-1 features. For genus-2 models, which present greater complexity, the DDPM-Polycube algorithm continues to perform effectively. In cases such as the Eight model (see Fig. 5) and Heart-glasses model (see Fig. 6), the algorithm successfully identifies the two holes and generates polycube structures where both the upper and lower parts feature holes aligned in the same direction.

We also test other complex genus-1 and genus-2 geometries to further evaluate the generalization capability of the algorithm. For the Plate-cleaner model (see Fig. 6), the algorithm generates a polycube structure where the upper part deforms into a cube and the lower part into a cube with a hole. For the Megaphone model (see Fig. 6), it identifies the cubes with holes in both the upper and lower parts, aligned in the same direction. In the No-bottom cup model (see Fig. 6), which has genus-2

topology, the algorithm generates two genus-1 cubes with perpendicular axes.

Overall, although our dataset only includes models from Type I to Type IX, the experimental results demonstrate that the DDPM-Polycube algorithm can generate polycube structures across a variety of complex geometric models, even recognizing topologies beyond its training range. The algorithm's ability to handle models with different genus levels and topological geometry without predefined polycube templates highlights its robustness and versatility. This makes it a valuable tool for polycube-based hexahedral mesh generation.

Remark 6 (Reasoning behind the model's effectiveness). *The model effectively uses the learned deformation capabilities of two geometric primitives: a cube and a cube with a hole. It identifies regions in the input geometry's point cloud that resemble these primitives in topology. These regions are then deformed into the corresponding structures. For example, cube-like areas are deformed into cube structures, while areas resembling a cube with a hole are deformed into cube with hole structures. By combining these learned geometric structures, the model generates new polycube structures, including complex CAD geometries with diverse topologies beyond its training range. This highlights the model's ability to process and generalize to complex geometric structures.*

5.3. Hex mesh generation and volumetric spline construction

After constructing the polycube structure, the next step is to generate hex meshes through surface segmentation and parametric mapping. Specifically, the surface segmentation ensures that the segmented regions align with the polycube structure, enabling a one-to-one correspondence between the surface of the CAD geometry and the surface of the polycube structure. This method, which performs segmentation after constructing the polycube structure, resolves the issues of traditional polycube methods, where segmentation or labeling often fails to ensure valid polycube structures. Since the segmentation or labeling in our method is inherently based on the polycube structure, it naturally guarantees the validity of the polycube structure. With the polycube structure serving as the parameter space, hex mesh generation is achieved through parametric mapping and octree subdivision. To further improve the quality of the hex mesh, post-processing techniques such as smoothing, pillowing, and optimization are applied. These techniques enhance the aspect ratio, reduce element distortion, and ensure that the mesh quality meets the requirements for IGA. Fig. 7 shows the polycube structures, all-hex meshes, and scaled Jacobian histograms for the Dice, Old Man, Ring, Rod, Lantern, and Eight models. The obtained all-hex meshes exhibit good quality (minimal Jacobian > 0.27).

Once a high-quality hex mesh is obtained, we test these models for IGA using TH-spline3D. The results of the spline construction exhibit C^0 -continuity around extraordinary points and edges, while maintaining C^2 -continuity in all other regions. Subsequently, Bézier elements are extracted for IGA analysis. For each tested model, we used ANSYS-DYNA to perform

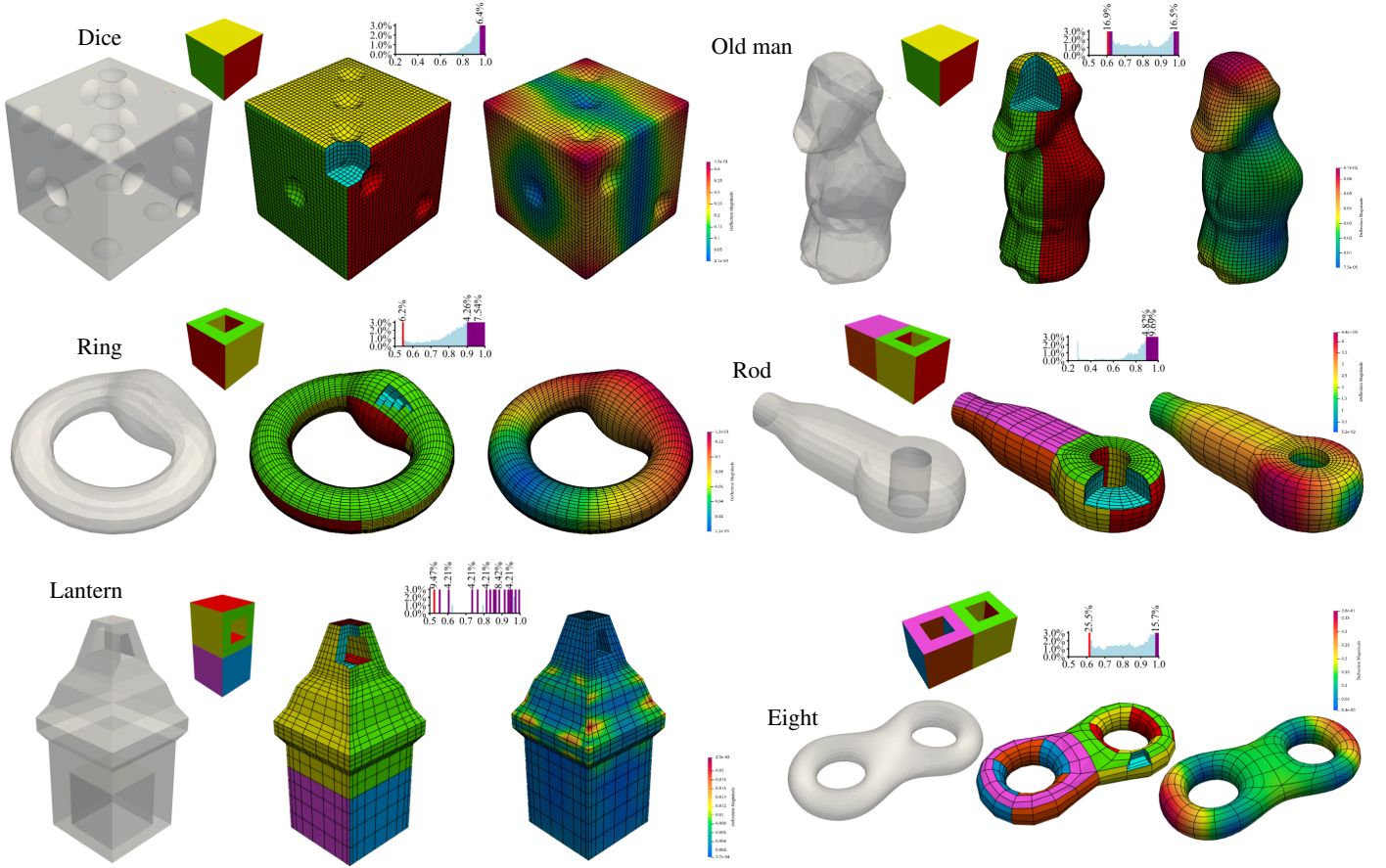


Figure 7: Results of the Dice, Old man, Ring, Rod, Lantern, and Eight models, including their polycube structures, all-hex control meshes (some elements are removed to show the interior), scaled Jacobian histograms, and volumetric splines with IGA eigenvalue analysis in ANSYS-DYNA. The red bar in the histograms represents the minimum scaled Jacobian. The number of vertices and the number of elements for these six models are (35,937, 32,768), (23,395, 20,992), (22,592, 20,480), (4,520, 3,840), (3,348, 2,565), and (1,253, 992), respectively.

eigenvalue analysis and present the results of one mode (see Fig. 7).

6. Conclusions and future work

This paper proposes a novel diffusion-based deep learning method, DDPM-Polycube, for generating high-quality hex meshes and constructing volumetric splines. By utilizing the improved DDPM, our method models the deformation from input geometry to polycube structures as a denoising task. This method eliminates the dependency of DL-Polycube algorithms on predefined polycube templates, enabling better generalization to complex geometries and diverse topologies. Experimental results demonstrate that DDPM-Polycube can generate valid polycube structures for complex engineering geometries and further use them to construct high-quality hex meshes and volumetric splines that meet the requirements of IGA. Additionally, the integration of DDPM-Polycube with mesh quality improvement techniques and TH-spline3D further enhances the automation of the process from B-Rep geometry to volumetric parameterization.

While the DDPM-Polycube algorithm represents an improvement on hex mesh generation and volumetric spline con-

struction, there are several areas for future improvement. First, the current algorithm primarily focuses on simple genus-0, genus-1, and genus-2 geometries. Extending the model to handle higher-genus and more complex geometries is an interesting research direction. Second, while the method can generate valid polycube structures, there is still room for improvement in deformation modeling and noise parameterization. Since the generated polycube structures carry non-standard Gaussian noise, we adopt volume-preserving Laplacian smoothing, a feature provided by the 3D graphics software Blender. However, for complex geometries, more efficient algorithms are needed to transform polycube structures with Gaussian noise into regular polycube structures. Third, the dataset used to train the DDPM-Polycube model includes only a limited set of geometric primitives. Expanding the dataset to incorporate more types of geometric primitives could significantly improve the model's robustness and generalization capability. Fourth, we observe during research that the algorithm has the ability to decompose geometries into geometric primitives. This feature has potential applications in another branch of IGA, namely volumetric parameterization based on CSG. Fifth, the application of context in this method is particularly important. If geometric information, connectivity relationships, or even basic data such

as STL files could replace the current context, it would bring the method closer to full automation. Furthermore, combining more multimodal learning frameworks could also further enhance the performance of DDPM-PolyCube. Finally, although this study primarily focuses on hex mesh generation, applying diffusion-based generative models to other types of meshes (such as hybrid meshes or hex-dominant meshes) could broaden the scope of this method. Moreover, extending the framework to support direct integration with CAD environments and automated IGA workflows could significantly improve its practical usability in real-world engineering applications. By addressing these challenges, we believe that DDPM-PolyCube has the potential to advance the fields of computational geometry, mesh generation, and IGA.

References

- [1] T. J. R. Hughes, J. A. Cottrell, Y. Bazilevs, Isogeometric analysis: CAD, finite elements, NURBS, exact geometry, and mesh refinement, *Computer Methods in Applied Mechanics and Engineering* 194 (2005) 4135–4195.
- [2] B. Zuo, Z. Huang, Y. Wang, Z. Wu, Isogeometric analysis for CSG models, *Computer Methods in Applied Mechanics and Engineering* 285 (2015) 102–124.
- [3] B. Li, X. Li, K. Wang, H. Qin, Generalized polycube trivariate splines, *Shape Modeling International Conference* (2010) 261–265.
- [4] Y. Zhang, W. Wang, T. J. Hughes, Solid T-spline construction from boundary representations for genus-zero geometry, *Computer Methods in Applied Mechanics and Engineering* 249–252 (2012) 185–197.
- [5] S. E. Benzley, E. Perry, K. Merkley, B. Clark, G. Sjaardama, A comparison of all hexagonal and all tetrahedral finite element meshes for elastic and elasto-plastic analysis, *4th International Meshing Roundtable* 17 (1995) 179–191.
- [6] M. Frâncu, A. Asgeirsson, K. Erleben, M. J. Rønnow, Locking-proof tetrahedra, *ACM Transactions on Graphics* 40 (2) (2021) 1–17.
- [7] N. Pietroni, M. Campen, A. Sheffer, G. Cherchi, D. Bommes, X. Gao, R. Scateni, F. Ledoux, J. Remacle, M. Livesu, Hex-mesh generation and processing: A survey, *ACM Transactions on Graphics* 42 (2) (2023) 1–44.
- [8] Y. J. Zhang, *Geometric Modeling and Mesh Generation from Scanned Images*, Chapman and Hall/CRC, 2016.
- [9] Y. J. Zhang, Challenges and advances in image-based geometric modeling and mesh generation, *Image-Based Geometric Modeling and Mesh Generation* (2013) 1–10.
- [10] D. Eppstein, Linear complexity hexahedral mesh generation, *Proceedings of the 12th Annual Symposium on Computational Geometry* (1996) 58–67.
- [11] Y. J. Zhang, Y. Bazilevs, S. Goswami, C. L. Bajaj, T. J. R. Hughes, Patient-specific vascular NURBS modeling for isogeometric analysis of blood flow, *Computer Methods in Applied Mechanics and Engineering* 196 (29–30) (2007) 2943–2959.
- [12] Y. Yu, Y. J. Zhang, K. Takizawa, T. E. Tezduyar, T. Sasaki, Anatomically realistic lumen motion representation in patient-specific space-time isogeometric flow analysis of coronary arteries with time-dependent medical-image data, *Computational Mechanics* 65 (2) (2020) 395–404.
- [13] J. Qian, Y. J. Zhang, Automatic unstructured all-hexahedral mesh generation from B-Reps for non-manifold CAD assemblies, *Engineering with Computers* 28 (4) (2012) 345–359.
- [14] R. Schneiders, A grid-based algorithm for the generation of hexahedral element meshes, *Engineering with Computers* 12 (3–4) (1996) 168–177.
- [15] J. Qian, Y. Zhang, W. Wang, A. C. Lewis, M. A. S. Qidwai, A. B. Geltmacher, Quality improvement of non-manifold hexahedral meshes for critical feature determination of microstructure materials, *International Journal for Numerical Methods in Engineering* 82 (11) (2010) 1406–1423.
- [16] M. Tarini, K. Hormann, P. Cignoni, C. Montani, Polycube-maps, *ACM Transactions on Graphics* 23 (3) (2004) 853–860.
- [17] H. Wang, Y. He, X. Li, X. Gu, H. Qin, Polycube splines, *Symposium on Solid and Physical Modeling* (2007) 241–251.
- [18] W. Wang, Y. J. Zhang, L. Liu, T. J. R. Hughes, Trivariate solid T-spline construction from boundary triangulations with arbitrary genus topology, *Computer Aided Design* 45 (2) (2013) 351–360.
- [19] K. Hu, Y. J. Zhang, Centroidal Voronoi tessellation based polycube construction for adaptive all-hexahedral mesh generation, *Computer Methods in Applied Mechanics and Engineering* 305 (2016) 405–421.
- [20] Y. Yu, X. Wei, A. Li, J. Liu, J. He, Y. J. Zhang, HexGen and Hex2Spline: Polycube-based hexahedral mesh generation and spline modeling for isogeometric analysis applications in LS-DYNA, *Springer INdAM Series: Proceedings of INdAM Workshop “Geometric Challenges in Isogeometric Analysis.”* (2022) 333–363.
- [21] M. Nieser, U. Reitebuch, K. Polthier, Cubecover - parameterization of 3D volumes, *Computer Graphics Forum* 30 (5) (2011) 1397–1406.
- [22] Y. Li, Y. Liu, W. Xu, W. Wang, B. Guo, All-hex meshing using singularity-restricted field, *ACM Transactions on Graphics* 31 (6) (2012) 1–11.
- [23] J. Lin, X. Jin, Z. Fan, C. Wang, Automatic polycube-maps, *Advances in Geometric Modeling and Processing* 4975 (2008) 3–16.
- [24] K. Hu, Y. Zhang, T. Liao, Surface segmentation for polycube construction based on generalized centroidal Voronoi tessellation, *Computer Methods in Applied Mechanics and Engineering* 316 (2017) 280–296.
- [25] H. Guo, X. Liu, D. Yan, Y. Liu, Cut-enhanced polycube-maps for feature-aware all-hex meshing, *ACM Transactions on Graphics* 39 (4) (2020) 1–14.
- [26] B. Li, X. Li, K. Wang, H. Qin, Surface mesh to volumetric spline conversion with generalized polycubes, *IEEE Transactions on Visualization and Computer Graphics* 99 (2013) 1–14.
- [27] X. Wei, Y. Zhang, T. J. R. Hughes, Truncated hierarchical tricubic C⁰ spline construction on unstructured hexahedral meshes for isogeometric analysis applications, *Computers and Mathematics with Applications* 74 (9) (2017) 2203–2220.
- [28] G. Xu, B. Li, L. Shu, L. Chen, J. Xu, T. Khajah, Efficient r-adaptive isogeometric analysis with Winslow’s mapping and monitor function approach, *Journal of Computational and Applied Mathematics* 351 (2019) 186–197.
- [29] Y. Siddiqui, A. Alliegro, A. Artemov, T. Tommasi, D. Sirigatti, V. Rosov, A. Dai, M. Nießner, MeshGPT: Generating triangle meshes with decoder-only transformers, *IEEE/CVF Conference on Computer Vision and Pattern Recognition* (2024) 19615–19625.
- [30] J. Gao, W. Chen, T. Xiang, A. Jacobson, M. McGuire, S. Fidler, Learning deformable tetrahedral meshes for 3D reconstruction, *Advances in Neural Information Processing Systems* 33 (2020) 9936–9947.
- [31] Y. Chen, T. He, D. Huang, W. Ye, S. Chen, J. Tang, X. Chen, Z. Cai, L. Yang, G. Yu, G. Lin, C. Zhang, MeshAnything: Artist-created mesh generation with autoregressive transformers, *arXiv:2406.10163* (2024) 1–19.
- [32] H. Tong, K. Qian, E. Halilaj, Y. J. Zhang, SRL-assisted AFM: Generating planar unstructured quadrilateral meshes with supervised and reinforcement learning-assisted advancing front method, *Journal of Computational Science* 72 (2023) 102109.
- [33] Y. Yu, Y. Fang, H. Tong, Y. J. Zhang, DL-PolyCube: Deep learning enhanced polycube method for high-quality hexahedral mesh generation and volumetric spline construction, *arXiv:1609.02907* (2024) 1–35.
- [34] I. Sutskever, O. Vinyals, Q. V. Le, Sequence to sequence learning with neural networks, *Advances in Neural Information Processing Systems* 27 (2014) 3104–3112.
- [35] I. Goodfellow, P. A. Jean, M. Mirza, B. Xu, W. F. David, S. Ozair, A. Courville, Y. Bengio, Generative adversarial nets, *Advances in Neural Information Processing Systems* 28 (2014) 2672–2680.
- [36] L. Dinh, S. D. Jascha, S. Bengio, Density estimation using Real NVP, *arXiv:1605.08803* (2016) 1–32.
- [37] D. P. Kingma, P. Dhariwal, Glow: Generative flow with invertible 1x1 convolutions, *Advances in Neural Information Processing Systems* 32 (2018) 10236–10245.
- [38] D. P. Kingma, M. Welling, Auto-encoding variational bayes, *arXiv:1312.6114* (2013) 1–14.
- [39] S. D. Jascha, E. Weiss, N. Maheswaranathan, S. Ganguli, Deep unsupervised learning using nonequilibrium thermodynamics, *International Conference on Machine Learning* (2015) 2256–2265.
- [40] J. Ho, A. Jain, P. Abbeel, Denoising diffusion probabilistic models, *Advances in Neural Information Processing Systems* 33 (2020) 6840–6851.
- [41] Y. Song, S. D. Jascha, D. P. Kingma, A. Kumar, S. Ermon, B. Poole,

Score-based generative modeling through stochastic differential equations, arXiv:2011.13456 (2020) 1–36.

- [42] A. Q. Nichol, P. Dhariwal, Improved denoising diffusion probabilistic models, International Conference on Machine Learning (2021) 8162–8171.
- [43] M. S. Floater, Parametrization and smooth approximation of surface triangulations, Computer Aided Geometric Design 14 (3) (1997) 231–250.
- [44] Y. Zhang, C. L. Bajaj, G. Xu, Surface smoothing and quality improvement of quadrilateral/hexahedral meshes with geometric flow, Communications in Numerical Methods in Engineering 25 (1) (2009) 1–18.
- [45] H. Tong, E. Halilaj, Y. J. Zhang, HybridOctree_hex: Hybrid octree-based adaptive all-hexahedral mesh generation with Jacobian control, Journal of Computational Science 78 (2024) 102278.
- [46] CMU-CBML, HexGen and Hex2Spline: Polycube-based hexahedral mesh generation and spline modeling for isogeometric analysis applications in LS-DYNA, https://github.com/CMU-CBML/HexGen_Hex2Spline.git (2024).
- [47] Y. Zhang, C. Bajaj, Adaptive and quality quadrilateral/hexahedral meshing from volumetric data, Computer Methods in Applied Mechanics and Engineering 195 (9-12) (2006) 942–960.